RSC Advances

Strong Addition Effect of Charge-Bridging Polymer in Polymer:Fullerene Solar Cells with Low Fullerene Contents

Journal:	*RSC Advances*
Manuscript ID:	RA-ART-03-2014-001918.R1
Article Type:	Paper
Date Submitted by the Author:	22-Apr-2014

Complete List of Authors:	Nam, Sungho; Kyungpook National University, Department of Chemical Engineering Park, Soohyeong; Kyungpook National University, Department of Chemical Engineering Kim, Hwajeong; Kyungpook National University, Department of Chemical Engineering Kim, YoungKyoo; Kyungpook National University, Department of Chemical Engineering

RSC Advances

RSCPublishing

ARTICLE

Strong Addition Effect of Charge-Bridging Polymer in Polymer:Fullerene Solar Cells with Low Fullerene Contents

Cite this: DOI: 10.1039/x0xx00000x

Received 00th March 2014,
Accepted 00th March 2014

DOI: 10.1039/x0xx00000x

www.rsc.org/

Sungho Nam,[a] Soohyeong Park,[b] Hwajeong Kim,[a,c] and Youngkyoo Kim,[a]*

We report a strong influence of charge-bridging polymer addition on the performance of polymer:fullerene solar cells with a low fullerene content, which were fabricated with bulk heterojunction (BHJ) films of poly(3-hexylthiophene) (P3HT) and [6,6]-phenyl-C_{61}-butyric acid methyl ester ($PC_{61}BM$). Poly[(4,8-bis-(2-ethylhexyloxy)-benzo[1,2-b:4,5-b']dithiophene)-2,6-diyl-alt-(N-2-ethylhexylthieno[3,4-c]pyrrole-4,6-dione)-2,6-diyl]] (PBDTTPD) was employed as a charge-bridging polymer by considering its energy band structure, while the $PC_{61}BM$ content was fixed as 33.3 wt.% (P3HT:$PC_{61}BM$ = 1:0.5 by weight). Results showed that the power conversion efficiency (PCE) of solar cells was greatly improved by more than 7-fold by adding 20 wt.% PBDTTPD but slightly decreased by further PBDTTPD addition. This huge PCE enhancement has been assigned to the charge-bridging role of PBDTTPD between P3HT and $PC_{61}BM$ domains, which is closely related to the pronounced nanostructure changes in the BHJ films including the increased size of $PC_{61}BM$ aggregates (~8.5 nm).

1. Introduction

The performance of polymer:fullerene solar cells has been greatly improved by employing new conjugated polymers and optimizing device structures since early breakthroughs for bulk heterojunction (BHJ) solar cells.[1-15] To date, the highest power conversion efficiency (PCE) has reached ~9.2% for single stack polymer:fullerene solar cells and ~10.6% for tandem polymer:fullerene solar cells.[12,13] The improved performance can be attributed primarily to the enhanced open circuit voltage (V_{OC}) due to the high-lying highest occupied molecular orbital (HOMO) energy levels of new conjugated polymers, while the enhanced light harvesting effect can be additionally counted because of their extended optical absorption ranges toward near infrared wavelengths.[10-15]

However, the stability (lifetime) of polymer:fullerene solar cells is still a big challenging point even though new conjugated polymers could deliver such high PCEs. Several reasons have been suggested for the low stability of polymer:fullerene solar cells, which include the corrosion effect by the acidity of hole-collecting buffer layers, the interfacial degradation between active layers and metal electrodes, the light-induced degradation of conjugated polymers (excited states), the gradual demixing between conjugated polymers and soluble fullerenes, etc.[16-24] Of such reasons, both the degradation of conjugated polymers and the demixing between conjugated polymers and fullerenes (morphological instability) under continuous solar light illumination may be the most challenging parts in order to secure the stability of polymer-based solar cells.

The demixing phenomenon between conjugated polymers and fullerenes can be assigned to the intrinsic nature of fullerenes that are basically small molecules with a tendency to undergo crystallization once an activation energy such as solar light is given.[18,25-29] Hence, to minimize the influence of the morphological instability owing to the phase demixing in the polymer:fullerene BHJ films, reducing the fullerene content can be one of the realistic approaches when it comes to the probability for the demixing events. However, the low fullerene content gives rise to poor device performances because of insufficient charge (electron) percolation paths generated in the BHJ films (active layers).[30-32] For example, the fullerene content should be higher than 0.7 part (ca. 41 wt.%) for poly(3-hexylthiophene) (P3HT) and [6,6]-phenyl-C_{61}-butyric acid methyl ester ($PC_{61}BM$) (i.e., P3HT:$PC_{61}BM$ = 1:0.7 by weight) in order to achieve a reasonable PCE (>2.5%).

Hence, in this work, we attempted to improve the performance of polymer:fullerene solar cells with a low fullerene content by adding a charge-bridging polymer to the polymer:fullerene BHJ films. Here we note that no attempt has been made to add charge-bridging polymers to the polymer:fullerene films with low fullerene contents, although various ternary blend approaches have been tried for typically high fullerene contents.[33-46] Here, as a model system, the P3HT:$PC_{61}BM$ (1:0.5 by weight - 33.3 wt.%) film was selected because the PCE of corresponding solar cells is as low as <0.5% compared to high PCE for typical P3HT:$PC_{61}BM$ solar cells with high $PC_{61}BM$ contents (>2.5% PCE depending on the supplier batches of P3HT materials). As the charge-bridging polymer, poly[(4,8-bis-(2-ethylhexyloxy)-benzo[1,2-b:4,5-

b']dithiophene)-2,6-diyl-alt-(N-2-ethylhexylthieno[3,4-c] pyrrole-4,6-dione)-2,6-diyl]] (PBDTTPD) was chosen because its band gap (1.8 eV) is close to that of the P3HT film (1.9 eV) so that we can minimize the influence of exciton (Förster) energy transfer from P3HT to the charge-bridging polymer in order to exactly investigate charge separation and transport effects inside the BHJ films.

2. Experimental Section

2.1 Materials and Solutions.

The P3HT polymer was purchased from Rieke Metal (regioregularity = 91%, weight-average molecular weight = 6.2×10^4 Da, polydispersity index = 2.32), while the PBDTTPD polymer (weight-average molecular weight = 13×10^4 Da, polydispersity index = 2.49) was supplied from Solarmer Materials, Inc. Note that the weight-average molecular weight and polydispersity index of PBDTTPD was measured by employing a gel permeation chromatography (GPC) in this work. $PC_{61}BM$ and PEDOT:PSS (solution, PH500) were purchased from Nano-C and H. C. Starck, respectively. The binary and ternary blend solutions were prepared using chlorobenzene as a solvent at a solid concentration of 15 mg/ml. The $PC_{61}BM$ content was fixed as 33.3 wt.%, while the weight ratio of P3HT and PBDTTPD was varied (the overall PBDTTPD content = 0, 1, 5, 10, 20, 40, 60 wt.%). The prepared binary and ternary blend solutions were subject to vigorous stirring on a hot plate (60 ^oC) for 24 h before spin-coating.

2.2 Thin film and Device Fabrication.

Prior to device fabrication, patterned indium-tin oxide (ITO)-coated glass substrates were cleaned using acetone and isopropyl alcohol in an ultrasonic cleaner, followed by drying with a nitrogen flow. The dried ITO-glass substrates were further cleaned inside UV-ozone chamber for 20 min in order to remove any remnant organic residues on the ITO surfaces. On top of the cleaned ITO-glass substrates, the PEDOT:PSS layer (thickness = 40 nm) was spin-coated and annealed at 200 ^oC for 15 min. Next, the binary and ternary blend layers were spin-coated on the PEDOT:PSS layer and soft-baked at 60 ^oC for 15 min, which led to the active layers (thickness = 60 nm). Then the film samples were transferred into a vacuum chamber equipped inside an argon-filled glove-box. After pumping down the pressure of vacuum chamber to ~1×10^{-6} Torr, lithium fluoride (LiF, thickness = ~1 nm) and aluminium (Al, thickness = 80 nm) were deposited on top of the active layers through a shadow mask. The device active area was 0.09 mm^2. All devices were subject to thermal annealing at 150 ^oC for 10 min and stored inside the same glove-box before measurement. The same film samples as prepared for the device fabrication were used for the AFM and GIXD measurements, while polymeric films were spin-coated on quartz substrates for the optical and photoelectron (PE) yield measurements. For the measurement of the electron mobility of the pristine PBDTTPD film, electron-only devices (ITO/PBDTTPD/Ca/Al) were fabricated by varying the thickness of the PBDTTPD layers. The thickness of calcium (Ca) and aluminium (Al) electrodes was 20 nm and 80 nm, respectively. The resulting electron mobility of the PBDTTPD films was 6.2×10^{-8} cm^2/Vs, which was obtained by applying a space charge limited current (SCLC) model for the current-voltage characteristics of electron-only devices.

2.3 Measurements.

The film thickness was measured using a thickness profiler (Alpha Step 200, Tencor Instruments). The optical absorption spectra of films were measured using a UV-visible spectrophotometer (Optizen 2120, MECASYS), while the PL spectra of films were measured with a fluorescence spectrometer (FS-2, SCINCO). The highest occupied molecular orbital (HOMO) energy level of the pristine P3HT and PBDTTPD films was calculated from the ionization potential that was measured using a photoelectron yield spectrometer (AC2, Riken-Keiki). The nanostructure of film samples was measured using a synchrotron radiation grazing incidence X-ray diffraction (GIXD) system (9A U-SAXS beamline, Pohang Accelerator laboratory, South Korea) (X-ray wavelength = 0.11 nm, incidence angle = 0.14^o) and field-emission transmission electron microscope (FE-TEM) (Titan G2 ChemiSTEM Cs Probe, FEI). The surface morphology of film samples was measured using an atomic force microscope (AFM, Nanoscope IIIa, Digital Instruments). The performance of solar cells was measured under 1 sun condition (100 mW/cm^2) using a specialized solar cell measurement system equipped with a solar simulator (92250A-1000, Newport-Oriel) and an electrometer (Model 2400, Keithley).

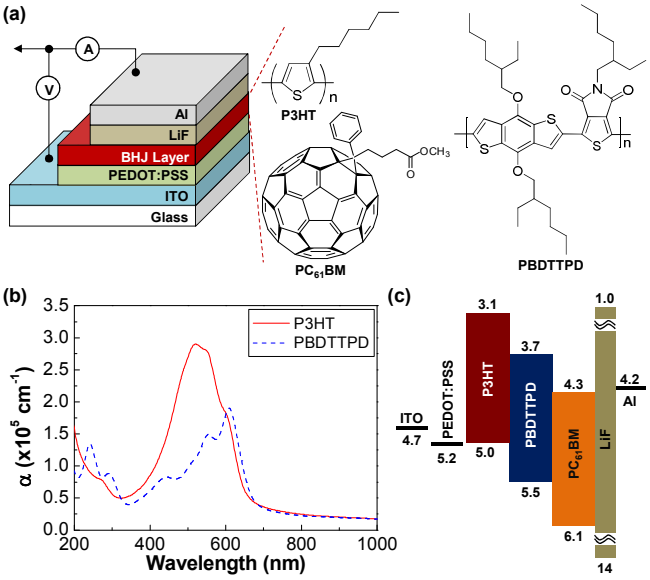

Fig. 1. (a) Illustration of device structure and materials used in this work. (b) Optical absorption coefficient (α) of P3HT and PBDTTPD films coated on quartz substrates. (c) Flat energy diagram for the solar cell illustrated in (a): Note that the energy unit (eV) and minus sign (-) were omitted in order to avoid crowding figures.

3. Results and Discussion

As shown in Fig. 1a, a normal type solar cell structure was employed for this research. Looking at the optical absorption spectra in Fig. 1b, the absorption edge is almost similar for the two polymers in the presence of considerably lower absorption coefficient (peak) for the PBDTTPD film than the P3HT film. Thus we can expect relatively small light-harvesting contribution of the PBDTTPD component compared to the P3HT component when the PBDTTPD content is low. Considering the flat energy band diagram in Fig. 1c (see also Fig. S1), the PBDTTPD component is likely to take electrons first from the P3HT component by charge separation process and then to deliver electrons to the $PC_{61}BM$ component by charge transport process (At the same time the hole transport may follow in the counter direction of the electron transport). In other words, the PBDTTPD component is supposed to play a

bridge role for charge transfer/transport between the P3HT component and the $PC_{61}BM$ component. We note that the PBDTTPD component itself can also absorb solar light and the photogenerated electrons can be transferred to the $PC_{61}BM$ component though the number of electrons is dependent on the PBDTTPD content (Similarly, the photogenerated holes in the PBDTTPD component can be transferred to the P3HT component).

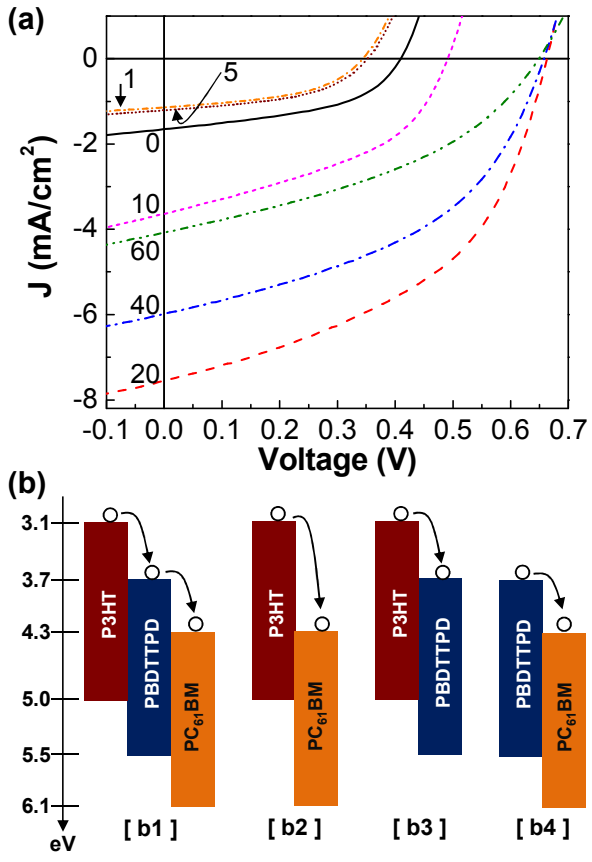

Fig. 2. (a) Light (100 mW/cm^2) J-V curves of devices according to the PBDTTPD content (the unit 'wt.%' is omitted). (b) Four different cases for possible charge separation (note that the minus sign '-' in the energy axis was omitted): (b1) cascade separation from P3HT to $PC_{61}BM$ via PBDTTPD, (b2) separation between P3HT and $PC_{61}BM$, (b3) separation between P3HT and PBDTT, (b4) separation between PBDTTPD and $PC_{61}BM$.

To investigate the influence of the PBDTTPD addition, the PDBTTPD content was varied up to 60 wt.% by fixing the weight ratio of P3HT and $PC_{61}BM$ ($PC_{61}BM$ = 33.3 wt.%). As observed from the current density – voltage (J-V) curves under solar light illumination (Fig. 2a), the P3HT:$PC_{61}BM$ solar cell without the PBDTTPD polymer resulted in very low short circuit current density (J_{SC} = 1.6 mA/cm^2) and V_{OC} (0.4 V) (see Table S1 and Fig. S2 for details). When a small amount of the PBDTTPD polymer (1 and 5 wt.%) was added, the light J-V curves became even worse leading to much lower J_{SC} and V_{OC}. However, interestingly, adding 10 wt.% PBDTTPD did greatly increase the J_{SC} (3.6 mA/cm^2) and V_{OC} (0.49 V) values. In particular, the J_{SC} and V_{OC} values reached ~7.6 mA/cm^2 and 0.66 V when the PBDTTPD content was 20 wt.%. Taking into account the almost 5-fold increased J_{SC} (from 1.6 mA/cm^2 to 7.6 mA/cm^2), we can briefly consider that the PBDTTPD component did play an efficient bridging role in transferring electrons from the P3HT component to the $PC_{61}BM$ component because only 20 wt.% PBDTTPD is too small to generate such high photocurrent when it comes to the quite low absorption coefficient as discussed in Fig. 1b. However, we need to pay our attention to the V_{OC} value (0.66 V), which is higher than typical V_{OC} (~0.62 V) for the best optimized P3HT:$PC_{61}BM$ solar cells using the present batch of P3HT (see Fig. S3a). This indicates that the PBDTTPD addition did additionally contribute to the increased V_{OC}, which is theoretically possible if the electrons in the PBDTTPD component are directly collected to the Al electrode (see Fig. 2b). However, as shown in Fig. S3, the performance of the P3HT:PBDTTPD solar cells is very poor so that the PBDTTPD component, as an electron acceptor, only cannot deliver such a high photocurrent. Hence we can expect a harmonic effect by both PBDTTPD and $PC_{61}BM$, which may be an enhanced electron transport for the PBDTTPD and $PC_{61}BM$ phases as evidenced from the noticeably (3-fold) reduced series resistance (R_S) from ~0.6 kΩ•cm^2 to ~0.2 kΩ•cm^2 (see Table S1). However, further increasing the PBDTTPD content did rather begin to reduce both J_{SC} and V_{OC} but the device performances of all ternary solar cells (P3HT:PBDTTPD:$PC_{61}BM$) fabricated here were still much better than the binary solar cells (P3HT:$PC_{61}BM$).

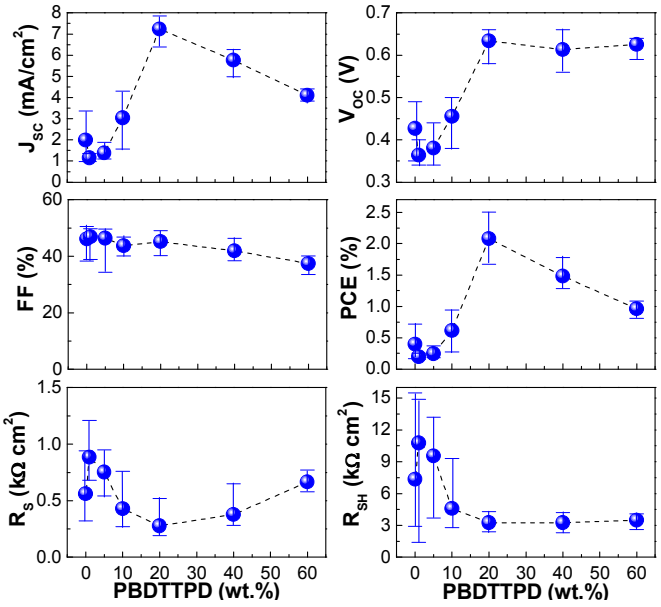

Fig. 3. Solar cell parameters (J_{SC}, V_{OC}, FF, PCE, R_S, R_{SH}) as a function of the PBDTTPD content: All data were taken from the light J-V curves in Fig. 2a.

The detailed trend of device performances is shown in Fig. 3. Here we find that the J_{SC} value was maximum at 20 wt.% PBDTTPD and then noticeably decreased by further increasing the PBDTTPD content, whereas the V_{OC} drop was relatively milder than the J_{SC} decrease. This result implies that the number of photogenerated charges was decreased by increasing the PBDTTPD content because of the low optical absorption coefficient of PBDTTPD (see Fig. 1b). The fill factor (FF) was not strikingly changed by the addition of PBTTTPD, but huge changes were made for R_S and shunt resistance (R_{SH}). Here the poor PCE by adding small amount of PBDTTPD (< 10 wt.%) can be ascribed to the increased R_S. From the present

PBDTTPD addition experiments, we achieved more than 7-fold improved PCE by adding 20 wt.% PBDTTPD.

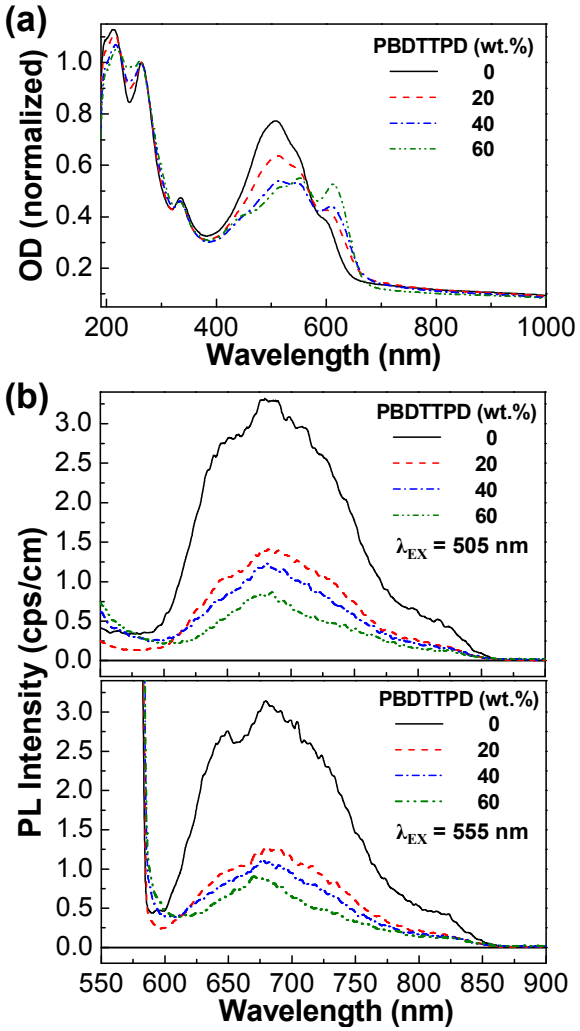

Fig. 4. (a) Wavelength-dependent optical density (OD, normalized at 264 nm) of the bulk heterojunction films according to the PBDTTPD content. (b) PL spectra of the bulk heterojunction films according to the PBDTTPD content by excitation at 505 nm (top panel) and 555 nm (bottom panel).

To understand the significantly improved device performance in detail, we have first investigated the optical absorption and photoluminescence (PL) spectra. As shown in Fig. 4a, the P3HT absorption part was decreased but the PBDTTPD absorption part was increased by increasing the PBDTTPD content. Considering that the solar light intensity is stronger at 500 nm (wavelength) than at 620 nm,[47] the number of photons absorbed by the binary blend film (P3HT:$PC_{61}BM$) is slightly higher than or similar to that by the ternary blend films (P3HT:PBDTTPD:$PC_{61}BM$) when it comes to the absorption area depending on the PBDTTPD contents. This result suggests that the light harvesting is not the reason for such huge increase in the J_{SC} value by adding the PBDTTPD polymer. Next, looking at the PL spectra (Fig. 4b), we find that the PL intensity was greatly reduced by adding the PBDTTPD polymer regardless of excitation wavelengths (we note that the thickness-normalized PL intensity was higher for the PBDTTPD polymer than the P3HT polymer as shown in Fig. S5). This result means that there was additional charge separation event between the P3HT component and the PBDTTPD component in addition to that between the P3HT component and the $PC_{61}BM$ component. In particular, the higher the PBDTTPD content, the lower the PL intensity. This result reflects that the charge separation (charge transfer from the P3HT component to the PBDTTPD component) became efficient as the PBDTTPD content increased, but it is opposite to the J_{SC} trend that was decreased as the PBDTTPD content increased further from 20 wt.% up to 60 wt.%. Therefore, we can shortly conclude that the charge (electron) transport may be a limiting factor at higher PBDTTPD contents as observed from the increased R_S values (see Fig. 3).

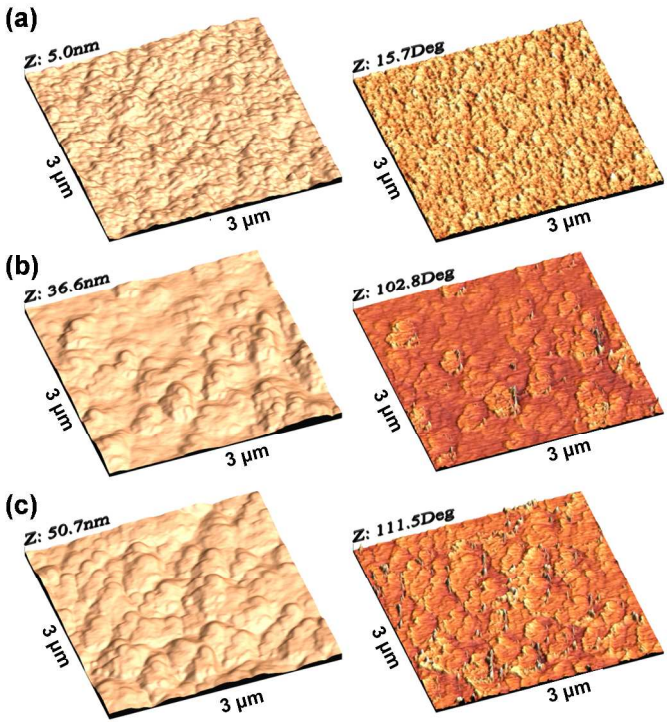

Fig. 5. AFM images (left: height mode; right: phase mode) of the bulk heterojunction films according to the PBDTTPPD content: (a) 0 wt.%, (b) 20 wt.%, (c) 40 wt.%. The root-mean-square (rms) roughness was (a) 0.57 nm, (b) 6.39 nm, (c) 8.32nm.

Next, we tried to examine the nanomorphology of the BHJ films according to the PBDTTPD content. As shown from the atomic force microscope (AFM) images in Fig. 5, the surface morphology became relatively coarser as the PBDTTPD content increased: The surface roughness was significantly increased from 0.57 nm (P3HT:$PC_{61}BM$) to 6.39 nm (P3HT:PBDTTPD:$PC_{61}BM$ at 20 wt.% PBDTTPD). This morphology change might contribute to making better charge percolation paths in the BHJ films, regarding the greatly enhanced J_{SC} by adding the PBDTTPD polymer. Interestingly, as shown from the transmission electron microscope (TEM) images in Fig. 6, the PBDTTPD addition changed not only the surface morphology but also the $PC_{61}BM$ segregation morphology inside the BHJ films from the dark areas in TEM images.[25,48]

As observed from the left side TEM images (low magnification) in Fig. 6, the apparent density (amount) of $PC_{61}BM$ molecules was increased as the PBDTTPD content increased. From the high magnification TEM images (right

side), we find that the size of the $PC_{61}BM$ aggregates became bigger for the ternary films (8.5~9 nm) than the binary film (~5 nm) (see also Fig. S6). These results reflect that the $PC_{61}BM$ molecules were slightly enriched toward the surface of films by the PBDTTPD addition leading to the formation of bigger $PC_{61}BM$ aggregates, which is partly responsible for the coarse morphology as observed from the AFM images.[45,49,50] Hence we think that the surface enrichment of $PC_{61}BM$ had a positive influence on the performance of the present normal type solar cells and the relatively bigger $PC_{61}BM$ aggregates by the presence of PBDTTPD did also help better electron transport.

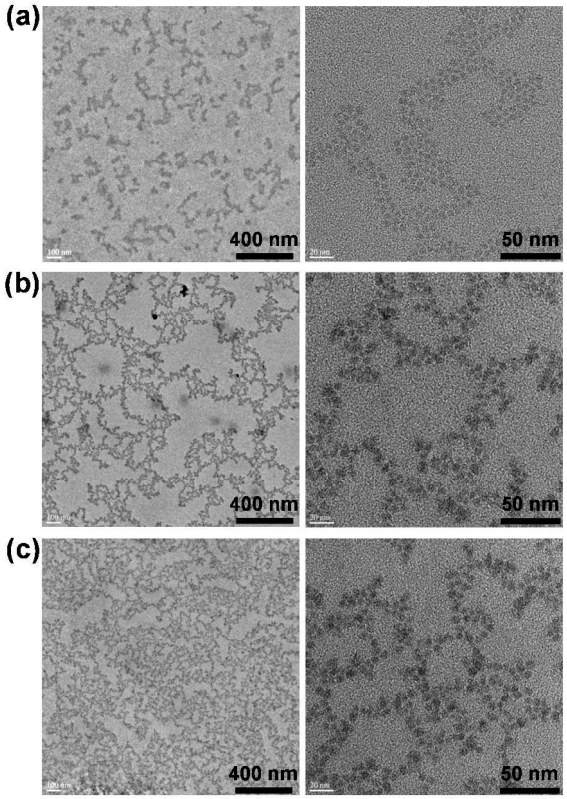

Fig. 6. TEM images of the bulk heterojunction films according to the PBDTTPPD content: (a) 0 wt.%, (b) 20 wt.%, (c) 40 wt.%. The magnification was 12k for left images and 100k for right images.

Considering the surface and internal segregation morphology changes in Fig. 5 and 6, we can expect that the molecular chain stacking in the BHJ films might be affected by the PBDTTPD addition. To examine this point, we performed the synchrotron radiation grazing incidence X-ray diffraction (GIXD) measurement for the binary and ternary blend films. As observed from the 2D GIXD images (Fig. 7a), the P3HT film showed typical Debye rings with high order diffractions up to (300) which are pronounced in the direction of out-of-plane (OOP).[51-55] However, the PBDTTPD film showed only (100) diffraction ring but no clear higher order diffractions,[56,57] which is clearly observed from the 1D profiles in Fig. 7b. This result indicates that the PBDTTPD polymer is less crystalline than the P3HT polymer. As expected, the high order diffraction feature of the P3HT component in the BHJ films was weakened as the PBDTTPD content increased. In addition, we find that the (100) peak position was obviously moved toward lower diffraction angles (from 2θ = 3.78o to 2θ = 3.40o) by adding only 20 wt.% PBDTTPD. This result implies that only 20 wt.% PBDTTPD addition did significantly change the P3HT chain stacking, which is again closely related with the huge change in the surface and internal segregation morphology as discussed in Fig.s 5 and 6. As a result, the d-spacing for molecular chain stacking became larger for the ternary blend films (~1.85 nm) than the binary blend film (~1.65 nm) (see Table S2). However, interestingly, the bigger d-spacing did not negatively but positively affect the device performance. This result may reflect that the devices with low fullerene contents are strongly influenced by the proper functioning of electron-accepting components (PBDTTPD and $PC_{61}BM$) rather than electron-donating (p-type) component (P3HT) in a viewpoint of relative energy band levels.

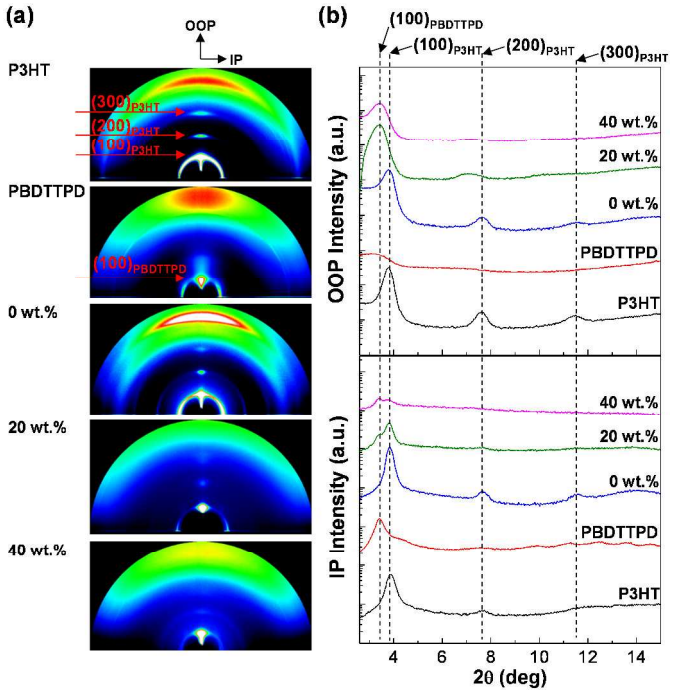

Fig. 7. (a) 2D GIXD images and (b) 1D GIXD profiles (top: OOP, bottom: IP) for the pristine (P3HT and PBDTTPD) films and the bulk heterojunction films with three different PBDTTPD contents. The major diffraction peaks for each polymer are marked on the top part of (b).

Finally, we have briefly examined the stability of the present solar cells before and after the PBDTTPD addition. First, the initial performance change was investigated by exposing devices under 1 sun (100 mW/cm^2) condition for 10 h. As shown from the J-V curves in Fig. 8a, all devices showed gradually decreased J_{SC} but the V_{OC} reduction was relatively small. Interestingly, the V_{OC} change was relatively stable for the ternary solar cells compared to the binary solar cell (we note that the binary solar cell showed on-going V_{OC} decreasing trend whereas the V_{OC} value seems to be levelled off for the ternary solar cells). Although the J_{SC} drop was relatively larger for the ternary solar cell with 20 wt.% PBDTTPD, the PCE was still much higher for the ternary solar cell with 20 wt.% PBDTTPD than the binary solar cell even after 10 h test. In addition, the ternary solar cell with 40 wt.% PBDTTPD exhibited quite stable PCE (only 0.14% PCE decrease after 10 h). Next, we tried to thermally treat the devices, which were exposed to the 1 sun condition for 10 h, at 100 ^oC for 1 h. As shown in Fig. 9, the performance of all devices was improved

by thermal annealing. However, the extent of performance recovery was more pronounced for the ternary solar cells (20 wt.% PBDTTPD: from PCE = 1.75% to 1.95%; 40 wt.% PBDTTPD: from PCE = 1.40% to 1.50%) than the binary solar cell (from PCE = 0.56% to 0.61%). Considering the initial stability change and the recovery trend by thermal treatment, the PBDTTPD addition is considered as an effective approach to improve both stability and efficiency in polymer:fullerene solar cells with low fullerene contents.

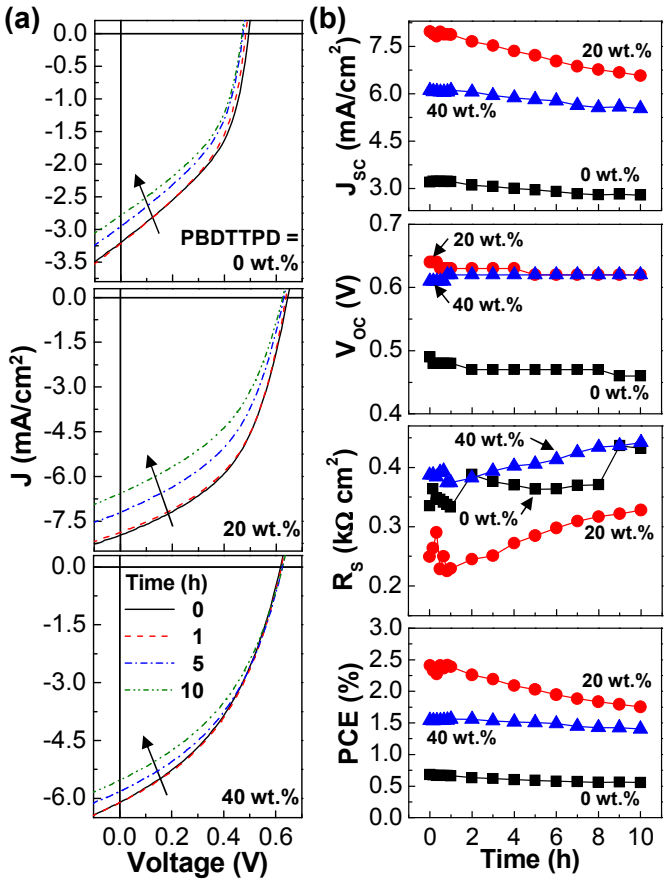

Fig. 8. (a) Change of light J-V curves for the devices with three different PBDTTPD contents according to the continuous illumination time under 1 sun condition (100 mW/cm^2). (b) Variation of J_{SC}, V_{OC}, R_S, and PCE as a function of illumination time for the devices with three different PBDTTPD contents.

4. Conclusions

The charge-bridging polymer, PBDTTPD, was added to the P3HT:$PC_{61}BM$ films with low $PC_{61}BM$ content (33.3 wt.%) of which solar cells show only ~0.3% PCE. At the low PBDTTPD contents less than 10 wt.% the device performance became slightly worse than the control device (P3HT:$PC_{61}BM$), but it was noticeably improved by further addition of PBDTTPD. When 20 wt.% PBDTTPD was added, the PCE reached ~2.4% which is more than 7-fold enhanced PCE. Further addition of PBDTTPD (40 wt.% and 60 wt.%) did slightly degrade the device performances but the resulting PCE values were still higher than the binary solar cell (P3HT:$PC_{61}BM$). This remarkably enhanced performance has been assigned to the bridging role of PBDTTPD for efficient charge transfer/transport between P3HT and $PC_{61}BM$ domains. The morphology measurements showed that the PBDTTPD addition induced the enrichment of $PC_{61}BM$ molecules toward the film surfaces (the $PC_{61}BM$ aggregates became bigger) leading to better vertical alignment of p-n junctions. In particular, it is very interesting that the device performance was significantly enhanced even though the P3HT stacking was considerably destroyed by adding 20 wt.% PBDTTPD as evidenced from the GIXD measurement. The initial stability test showed that the PCE of the ternary solar cells with the PBDTTPD polymer was still higher than the binary solar cell even after 10 h illumination of simulated solar light. In addition, the performance of the ternary solar cell with 20 wt.% PBDTTPD, which was exposed to 1 sun condition for 10 h, was relatively well recovered by thermal treatment, though other devices did also show similar recovery trend.

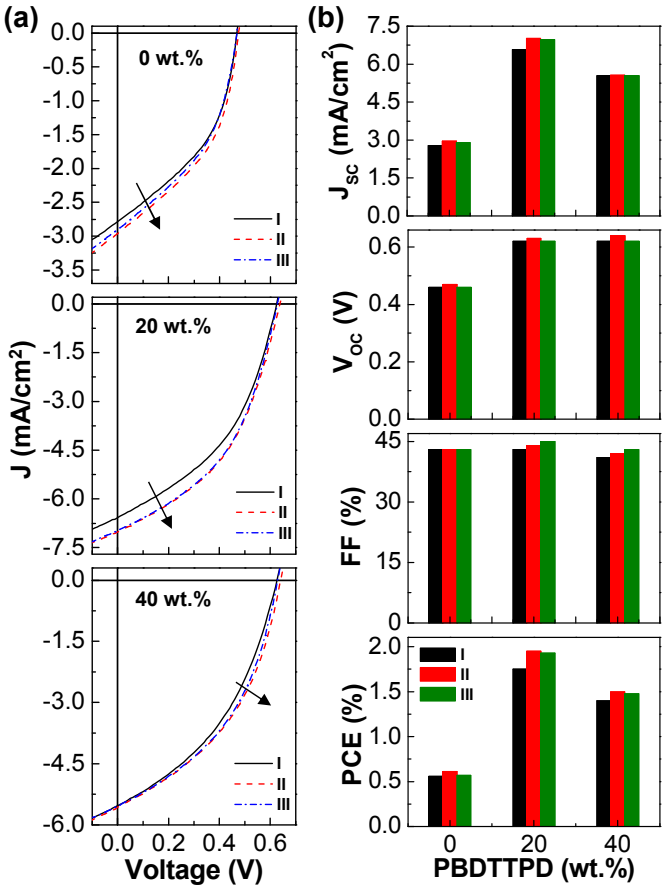

Fig. 9. (a) Change of light J-V curves for the devices with three different PBDTTPD contents: (I) After 10 h exposure to 1 sun condition (100 mW/cm^2), (II) thermal treatment for the devices 'I' at 100 °C for 1 h, (III) 10 h exposure to 1 sun condition for the devices 'II'. (b) Variation of J_{SC}, V_{OC}, FF, and PCE for the devices with three different PBDTTPD contents according to the treatment conditions (I, II, III).

Acknowledgements

This work was financially supported by Korean Government grants (Basic Research Laboratory Program_2011-0020264, Pioneer Research Center Program_2012-0001262, Basic Science Research Program_2009-0093819,

NRF_2012R1A1B3000523, NRF_2012K1A3A1A09027883, NRF_2013M4A1039332, NRF_2012056848).

Notes and references

[a]Organic Nanoelectronics Laboratory, Department of Chemical Engineering, Kyungpook National University, Daegu 702-701, Republic of Korea.
[b]Composite Material Development 1 Group, Advanced Composite Materials Technical Centre, Toray Advanced Materials Korea Inc, Gumi 730-410, Republic of Korea.
[c]Research Institute of Advanced Energy Technology, Kyungpook National University, Daegu 702-701, Republic of Korea.

*Corresponding author: Prof. Youngkyoo Kim.
Email) ykimm@knu.ac.kr
Tel) +82-53-950-5616

Electronic Supplementary Information (ESI) available: [Solar cell performance, d-spacings for pristine and BHJ films, PE yield spectra of P3HT and PBDTTPD films, semi-logarithmic J-V curves of devices, dark J-V curves of devices, light J-V curves of two binary BHJ devices, PL spectra of P3HT and PBDTTPD films, and enlarged TEM images]. See DOI: 10.1039/b000000x/

1 S. E. Shaheen, C. J. Brabec, N. S. Sariciftci, *Appl. Phys. Lett.*, 2001, **78**, 841.
2 F. Padinger, R. S. Rittberger, N. S. Sariciftci, *Adv. Funct. Mater.*, 2003, **13**, 85.
3 Y. Kim, S. A. Choulis, J. Nelson, D. D. C. Bradley, S. Cook, J. R. Durrant, *Appl. Phys. Lett.*, 2005, **86**, 063502.
4 W. Ma, C. Yang, X. Gong, K. Lee, A. J. Heeger, *Adv. Funct. Mater.*, 2005, **15**, 1617.
5 M. Reyes-Reyes, K. Kim, D. L. Carroll, *Appl. Phys. Lett.*, 2005, **87**, 083506.
6 T. Erb, U. Zhokhavets, G. Gobsch, S. Raleva, B. Stühn, P. Schilinsky, C. Waldauf, C. J. Brabec, *Adv. Funct. Mater.*, 2005, **15**, 1193.
7 G. Li, V. Shrotriya, J. S. Huang, Y. Yao, T. Moriarty, K. Emery, Y. Yang, *Nat. Mater.*, 2005, **4**, 864.
8 Y. Kim, S. Cook, S. M. Tuladhar, S. A. Choulis, J. Nelson, J. R. Durrant, D. D. C. Bradley, M. Giles, I. Mcculloch, C. S. Ha, M. Ree, *Nat. Mater.*, 2006, **5**, 197.
9 J. Y. Kim, K. Lee, N. E. Coates, D. Moses, T. Q. Nguyen, M. Dante, A. J. Heeger, *Science*, 2007, **317**, 222.
10 J. Peet, J. Y. Kim, N. E. Coates, W. L. Ma, D. Moses, A. J. Heeger, G. C. Bazan, *Nat. Mater.*, 2007, **6**, 4970.
11 H. Y. Chen, J. Hou, S. Zhang, Y. Liang, G. Yang, Y. Yang, L. Yu, Y. Wu, G. Li, *Nat. Photon.*, 2009, **3**, 649.
12 Z. He, C. Zhong, S. Su, M. Xu, H. Wu, Y. Cao, *Nat. Photon.*, 2012, **6**, 591.
13 J. You, L. Dou, K. Yoshimura, T. Kato, K. Ohya, T. Moriarty, K. Emery, C. C. Chen, J. Gao, G. Li, Y. Yang, *Nat. Commun.*, 2013, **4**, 1446.
14 W. Li, A. Furlan, K. H. Hendriks, M. M. Wienk, R. A. J. Janssen, *J. Am. Chem. Soc.*, 2013, **135**, 5529.
15 L. Dou, J. You, J. Yang, C. C. Chen, Y. He, S. Murase, T. Moriarty, K. Emery, G. Li, Y. Yang, *Nat. Photon.*, 2012, **6**, 180.
16 M. Jørgensen, K. Norrman, S. A. Gevorgyan, T. Tromholt, B. Andreasen, F. C. Krebs, Adv. Mater., 2012, **24**, 580.
17 K. Norrman, M. V. Madsen, S. A. Gevorgyan, F. C. Krebs, *J. Am. Chem. Soc.*, 2010, **132**, 16883.
18 H. Kim, M. Shin, J. Park, Y. Kim, *ChemSusChem*, 2010, **3**, 476-480.
19 H. Kim, S. Nam, H. Lee, S. Woo, C. S. Ha, M. Ree, Y. Kim, *J. Phys. Chem. C*, 2011, **115**, 13502.
20 S. Lee, S. Nam, H. Lee, H. Kim, Y. Kim, *ChemSusChem*, 2011, **4**, 1607.
21 X. Fan, G. Fang, F. Cheng, P. Qin, H. Huang, Y. Li, *J. Phys. D: Appl. Phys.*, 2013, **46**, 305106.
22 A. Kumar, R. Devine, C. Mayberry, B. Lei, G. Li, Y. Yang, *Adv. Funct. Mater.*, 2010, **20**, 2729.
23 Y. W. Soon, H. Cho, J. Low, H. Bronstein, I. McCulloch, J. R. Durrant, *Chem. Commun.*, 2013, **49**, 1291.
24 P. A. Cox, D. A. Waldow, T. J. Dupper, S. Jesse, D. S. Ginger, *ACS Nano*, 2013, **7**, 10405.
25 X. Yang, J. Loos, S. C. Veenstra, W. J. H. Verhees, M. M. Wienk, J. M. Kroon, A. J. Michels, R. A. J. Janssen, *Nano Lett.*, 2005, **5**, 579.
26 Y. Kim, J. Nelson, T. Zhang, S. Cook, J. R. Durrant, H. Kim, J. Park, M. Shin, S. Nam, M. Heeney, I. McCulloch, C. S. Ha, D. D. C. Bradley, *ACS Nano*, 2009, **3**, 2557.
27 H. Kim, M. Shin, J. Park, Y. Kim, *IEEE Trans. Nanotechnol.*, 2010, **9**, 400.
28 N. C. Miller, E. Cho, M. J. N. Junk, R. Gysel, C. Risko, D. Kim, S. Sweetnam, C. E. Miller, L. J. Richter, R. J. Kline, M. Heeney, I. McCulloch, A. Amassian, D. A. Feliz, C. Knox, M. R. Hansen, D. Dudenko, B. F. Chmelka, M. F. Toney, J. L. Brédas, M. M. McGehee, *Adv. Mater.*, 2012, **24**, 6071.
29 D. Gao, B. Djukic, W. Shi, C. R. Bridges, L. M. Kozycz, D. S. Seferos, *ACS Appl. Mater. Interfaces*, 2013, **5**, 8038.
30 Y. Kim, S. A. Choulis, J. Nelson, D. D. C. Bradley, S. Cook, J. R. Durrant, *J. Mater. Sci.*, 2005, **40**, 1371.
31 B. Kim, B. Ma, V. R. Donuru, H. Liu, J. M. J. Fréchet, *Chem. Commun.*, 2010, **46**, 4148.
32 A. Calabrese, A. Pellegrino, R. Po, A. Savoini, F. Tinti, N. Camaioni, *Sol. Energy Mater. Sol. Cells*, 2011, **95**, 3428.
33 Y. Kim, M. Shin, H. Kim, Y. Ha, C. S. Ha, *J. Phys. D: Appl. Phys.*, 2008, **41**, 225101.
34 H. Kim, M. Shin, Y. Kim, *J. Phys. Chem. C*, 2009, **113**, 1620.
35 C. H. Chen, C. H. Hsieh, M. Dubosc, Y. J. Cheng, C. S. Hsu, *Macromolecules*, 2010, **43**, 697.
36 S. J. Park, J. M. Cho, W. B. Byun, J. C. Lee, W. S. Shin, I. N. Kang, S. J. Moon, S. K. Lee, *J. Polym. Sci., Part A: Polym. Chem.*, 2011, **49**, 4416.
37 M. C. Chen, D. J. Liaw, Y. C. Huang, H. Y. Wu, Y. Tai, *Sol. Energy Mater. Sol. Cells*, 2011, **95**, 2621.
38 Z. Hu, S. Tang, A. Ahlvers, S. I. Khondaker, A. J. Gesquiere, *Appl. Phys. Lett.*, 2012, **101**, 053308.
39 Y. C. Wu, Y. H. Chao, C. L. Wang, C. T. Wu, C. S. Hsu, Y. L. Zeng, C. Y. Lin, *J. Polym. Sci., Part A: Polym. Chem.*, 2012, **50**, 5032.
40 T. Ameri, J. Min, N. Li, F. Machui, D. Baran, M. Forster, K. J. Schottler, D. Dolfen, U. Scherf, C. J. Brabec, *Adv. Energy Mater.*, 2012, **2**, 1198.
41 F. Machui, S. Rathgeber, N. Li, T. Ameri, C. J. Brabec, *J. Mater. Chem.*, 2012, **22**, 15570.

42 T. Ameri, T. Heumüller, J. Min, N. Li, G. Matt, U. Scherf, C. J. Brabec, *Energy Environ. Sci.*, 2013, **6**, 1796.
43 M. Koppe, H. J. Egelhaaf, E. Clodic, M. Morana, L. Lüer, A. Troeger, V. Sgobba, D. M. Guldi, T. Ameri, C. J. Brabec, *Adv. Energy Mater.*, 2013, **3**, 949.
44 H. L□slein, T. Ameri, G. J. Matt, M. Koppe, H. J. Egelhaaf, A. Troeger, V. Sgobba, D. M. Guldi, C. J. Brabec, *Macromol. Rapid Commun.*, 2013, **34**, 1090.
45 T. Ameri, P. Khoram, J. Min, C. J. Brabec, *Adv. Mater.*, 2013, **25**, 4245.
46 N. Li, P. Kubis, K. Forberich, T. Ameri, F. C. Krebs, C. J. Brabec, *Sol. Energy Mater. Sol. Cells*, 2014, **120**, 701
47 J. A. Duffie, Beckman, W. A. Solar Engineering of Thermal Processes, Wiley, Hoboken, NJ, USA, 2013
48 R. M. Beal, A. Stavrinadis, J. H. Warner, J. M. Smith, H. E. Assender, A. A. R. Watt, *Macromolecules*, 2010, **43**, 2343.
49 S. S. van Bavel, M. Bärenklau, G. de With, H. Hoppe, J. Loos, *Adv. Funct. Mater.*, 2010, **20**, 1458.
50 J. A. Renz, T. Keller, M. Schneider, S. Shokhovets, K. D. Jandt, G. Gobsch, H. Hoppe, *Sol. Energy Mater. Sol. Cells*, 2009, **93**, 508.
51 M. Shin, H. Kim, J. Park, S. Nam, K. Heo, M. Ree, C. S. Ha, Y. Kim, *Adv. Funct. Mater.*, 2010, **20**, 748.
52 S. Nam, M. Shin, H. Kim, C. S. Ha, M. Ree, Y. Kim, *Adv. Funct. Mater.*, 2011, **21**, 4527.
53 S. Nam, S. Lee, L. Lee, M. Shin, H. Kim, Y. Kim, *Nanoscale*, 2011, **3**, 4261.
54 H. Yang, T. J. Shin, L. Yang, K. Cho, C. Y. Ryu, Z. Bao, *Adv. Funct. Mater.*, 2005, **15**, 671.
55 N. D. Treat, M. A. Brady, G. Smith, M. F. Toney, E. J. Kramer, C. J. Hawker, *Adv. Energy Mater.*, 2011, **1**, 82.
56 C. Piliego, T. W. Holcombe, J. D. Douglas, C. H. Woo, P. M. Beaujuge, J. M. J. Fréchet, *J. Am. Chem. Soc.*, 2010, **132**, 7595.
57 C. Cabanetos, A. E. Labban, J. A. Bartelt, J. D. Douglas, W. R. Mateker, J. M. J. Fréchet, M. D. McGehee, P. M. Beaujuge, *J. Am. Chem. Soc.*, 2013, **135**, 4656.

[Graphic Abstract]

The efficieny of polymer:fullerene solar cells with low fullerene contents is significantly improved by adding a charge-bridging polymer.